Research Article | Vol. 27, No. 11 | 27 May 2019 | OPTICS EXPRESS 16080
Optics EXPRESS

# Comparison of femtosecond shadowgraphy and optical Kerr gated ballistic imaging for measurements of spray structures

MINGXIN WANG, JINHAI SI,* WENJIANG TAN, YIPENG ZHENG, AND YANG YANG

*Key Laboratory for Physical Electronics and Devices of the Ministry of Education, Shannxi Key Lab of Information Photonic Technique, School of Electronic and Information Engineering, Xi'an Jiaotong University, Xianning-xilu 28, Xi'an, 710049, China*
*jinhaisi@mail.xjtu.edu.cn

**Abstract:** Two femtosecond methods for imaging moderate liquid-gas sprays in the near-field region of spray nozzles — shadowgraphy and optical Kerr gated (OKG) ballistic imaging — were compared. Most spray structures can be captured using femtosecond shadowgraphy that can freeze the motion of the sprays. Femtosecond OKG ballistic imaging can distinguish finer structures and more-realistic liquid sheets by the filtering of multiple scattered photons. To compensate for the high-spatial-frequency components of the spray structures filtered by OKG ballistic imaging, differential OKG (DOKG) ballistic imaging was demonstrated. For dilute sprays, femtosecond shadowgraphy with a relatively simple experimental setup is recommended. For dense sprays, femtosecond OKG (or DOKG) ballistic imaging is more suitable.



## 1. Introduction

Liquid-gas mixed spray imaging has always been an important issue, because it is significant for the analysis of the combustion state of many combustion engines. The completeness, efficiency, and stability of combustion are largely related to fuel-oxidizer mixture preparation and, in particular, to rapid liquid breakup and atomization [1]. The size of the droplets broken from the liquid fuel will certainly affect the combustion situation. The fine droplets will evaporate fast and mix properly with air, which leads to its complete and proficient combustion. So understanding the structure and dynamics of the fuel sprays is critical in optimizing the jet parameters to increase fuel combustion efficiency and reduce pollutant emission [2,3]. At the exit of spray nozzle, intact liquid structures extrude into the gas phase and break up to "primary droplets" quickly via turbulence, cavitation, rapid development of surface-wave structures, other forms of shear, or a combination of these mechanisms [4]. This area where primary breakup occurs is called the "dense-spray" or "near-field" region. After that, the primary droplets undergo "secondary breakup," collide, and coalesce, forming a "dilute-spray" or "far-field" region. When a light beam is introduced into the spray, especially its near-field region, most photons are strongly scattered into various angles by the drops. These scattered photons undergo multiple light scatterings or a random walk in the scattering medium, losing information of liquid structures and providing severe background noise [5]. To improve the measurements of the flow structures in an optical dense spray, some scattered-light mitigation strategies are employed to filter the collected image signal [6]. Moreover, the spray structure evolved at a very high velocity in the near-field region. It will fail to avoid blurring of these high-speed spray structures by using an ordinary continuous light source and high-speed cameras because of the limited exposure time.

Optical Kerr gated (OKG) ballistic imaging is one excellent technique that can suppress significant image corruption caused by multiple light scatterings. It was introduced by Alfano's

#357303 https://doi.org/10.1364/OE.27.016080
Journal © 2019 Received 10 Jan 2019; revised 6 May 2019; accepted 8 May 2019; published 22 May 2019

Optics EXPRESS

group [7–9] and applied to spray diagnostics by Linne and his associates [10,11]. The OKG ballistic imaging utilized ultrashort laser pulses and an OKG activated optical shutter to suppress the influence of multiply scattered light and freeze the motion of the sprays [6]. It has been used to study a number of different sprays, e.g., a laminar water jet in a cross-flow of air [12,13], the liquid core in an atomizing diesel spray issuing into air at different pressures [14–16], a rocket injector [1,9], and an effervescent spray [13]. However, ultrafast high-repetition imaging of fuel sprays using a picosecond fiber laser has recently demonstrated that a high-quality spray image could be also obtained only by freezing the spray motion. Meyer and his associates did a comparative experiment of femtosecond OKG ballistic imaging and femtosecond shadowgraphy. The results showed that the femtosecond OKG ballistic imaging produced image contrast enhancement [1], in which the images were based on the statistical data separately obtained by using the two imaging approaches. To the knowledge of the authors of the present work, the comparative study of the imaging of spray structures using femtosecond shadowing and OKG ballistic-imaging techniques currently lacks direct experimental comparisons. Direct experimental comparisons might find the characteristics and application condition for these ultrafast imaging approaches.

In this study, femtosecond shadowgraphy and OKG ballistic imaging were demonstrated simultaneously in moderately dense liquid-gas sprays from an imitative rocket injector. The different details of spray structures in real time and application condition for the two ultrafast imaging approaches are discussed. Furthermore, a differential optical Kerr gated (DOKG) imaging was applied to liquid-gas sprays for overcoming the low-pass filtering influence induced by optical Kerr effect [17]. Detailed principle and experimental setup were introduced in the next part. The results show that DOKG imaging significantly improve the sharpness and the spatial resolution of the spray images.

## 2. Experimental details

A schematic of the imaging system is shown in Fig. 1. An amplified Ti:sapphire femtosecond laser system (Libra-USP-HE, Coherent Inc., USA) was used as the light source. It can generate ~120-fs, 3-mJ, and 800-nm laser pulses at a repetition rate of 1 kHz. As shown in Fig. 1, the laser beam was split into two parts by a 50/50 beam splitter (BS1). The transmitted part and the reflective part were used as the signal beam and the pump beam, respectively. The pump beam was filtered using a short-pass filter (SPF). A half-wave plate rotated the polarization of the pump beam by $\pi/4$ to obtain the maximum transmission efficiency. The pump beam passed through an optical delay line (ODL) used to control the time delay between the pump pulse and the signal pulse and then was focused on the optical Kerr medium with a size of 3.5 mm by lens L0 (focal length, $f_1$ = 400 mm). The OKG consisted of a pair of crossed Glan-Taylor polarizers P1 and P2 (PGT5012, Union Optic, Inc., China) and an optical Kerr medium (OKM) between them. The polarization direction of the polarizer P1 was horizontal, and the polarization direction of P2 in Fig. 1(a) was vertical. CS2 filled in a 5-mm-thickness quartz cuvette was used as the optical Kerr medium. The signal beam was modulated by the imaging object (resolution test target or spray). The imaging object could be a resolution test target (RT, RT-MIL-TP2001, Beijing Reallight Technology Co., Ltd., China) in front of the scattering medium (a suspension of polystyrene spheres with 3.13-μm diameters) or liquid-gas mixed spray. The signal beam was then focused by lens L1 (focal length, $f_2$ = 160 mm) into the OKM, overlapped with the pump light. The transmitted signal light was collected by lens L2 (focal length, $f_3$ = 200 mm). To perform femtosecond OKG imaging and ultrafast shadowgraphy simultaneously, part (a) was connected to the main light path, and part (a) would be replaced by part (b) if DOKG imaging results needed to be gathered. In the condition shown in Fig. 1(a), before passing through the polarizer P2, the light was split into two parts by a beam splitter (BS2). The transmitted part formed the OKG imaging and the reflective part formed the conventional femtosecond shadowgraphy. Both signal beams were imaged onto charge-coupled device cameras (CCD1 and CCD2, INFINITY3-1 M-NS-TPM, Lumenera Corporation, Ottawa,

Optics EXPRESS

Canada). The SPF in pump beam path and the long-pass filter (LPF) in front of CCD1 were used to decrease the noise generated by the pump pulse scattering in the OKM.

In the condition shown in Fig. 1(b), there were two more components arranged in the light path to perform DOKG imaging than in Fig. 1(a). First, the polarization directions of P3 and P4 were no longer perpendicular to P1. The angle between the polarization direction of P3 (or P4) and the vertical direction was rotated by a heterodyne angle. In a study, the heterodyne angels of P3 and P4 were set to –3° and + 3° to produce the negative heterodyne OKG signal and the positive heterodyne OKG signal, respectively. The heterodyne OKG signals carried all the spatial spectral components of the imaging object. DOKG images were acquired by subtracting the image with positive heterodyne signal from the image with a negative heterodyne signal, which removed the background light and compensated for high spatial frequency components. Second, a quarter-wave plate (λ/4) whose optical axis was parallel to the polarizer P1 was placed between the optical Kerr medium and the analyzer P2 to provide a π/2 optical phase bias. The phase bias could enhance the strength of heterodyned signals [18].

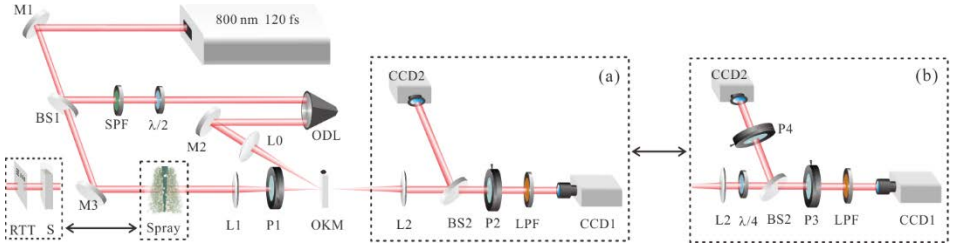


Fig. 1. Imaging system for simultaneously performing the femtosecond OKG imaging and femtosecond shadow imaging: imaging system of OKG (a) and DOKG (b) — M1, M2, M3: reflector; BS1, BS2: beam splitter; SPF: short-pass filter; λ/2: half-wave plate; ODL: optical delay line; L0, L1, L2: lenses; OKM: optical Kerr medium; RTT: resolution test target; S: scattering medium; P1, P2, P3, P4: polarizers; LPF: long-pass filter; λ/4: quarter-wave plate.

In the experiment, an imitative rocket injector was used to provide liquid-gas mixed sprays [1]. The nozzle was modified from a gas-centered swirl-coaxial injector configuration [19]. The liquid was metered using a rotameter with a range of 0.2 to 6 liters per minute (lpm) and ± 2.5% full-scale accuracy. The water is infused into an annular chamber along the outer diameter of the nozzle. When filling the chamber, the water is injected via four small holes that are tangent to the cavity into an internal cavity along the inner diameter of the nozzle. Air metered by a 200 lpm rotameter is pressed into the center of the nozzle by an air compressor and then presses the liquid layer along the wall out of the nozzle as liquid-gas mixed sprays. In the experiment, the exit diameter of this nozzle was 4.5 mm, and the flow rates of water and air were 1.35 lpm and 180 lpm, respectively.

## 3. Results and discussion

First, the performance of the imaging system in scattering environments was tested with a resolution test chart as the imaging object. In Fig. 2(a), the femtosecond shadowgraphy for the object is shown without a scattering medium as a reference image. Figures 2(b)-2(d) show the three ultrafast imaging methods for the object hidden in a suspension of polystyrene spheres as the scattering medium. Figure 2(b) shows that, in the image obtained using femtosecond shadowgraphy, the shadowed and unshadowed regions cannot be identified clearly, because it is seriously disturbed by multiple scattered photons. Figure 2(c) shows that the contrast of the OKG ballistic images is improved significantly by filtering multiple scattered photons. However, the boundaries of the resolution test patterns are slightly blurred, and the small targets are difficult to distinguish. The reason is that the gating beam induces a transient aperture in the Kerr material in the OKG ballistic imaging system, which filters some high-spatial-frequency components of the detected object. Therefore, the sharpness of the images and spatial resolution of the imaging system decrease [19]. To overcome the low-pass

Optics EXPRESS

spatial-filtering influence, we employed a femtosecond DOKG imaging method to compensate for the high spatial frequency components of the objects. The DOKG image was obtained by subtracting the positive heterodyne OKG image from the negative heterodyne OKG image, as described in the experimental section. The details about the DOKG method were given elsewhere [20]. As shown in Fig. 2(d), the smaller targets can be distinguished compared with that shown in Fig. 2(c).

To evaluate the performance of the imaging system quantitatively, the Modulation Transfer Function (MTF) and Point-Spread Function (PSF) of each experimental configuration were then calculated as shown in Fig. 2. The calculation methods of MTF and PSF are derived from the reference [10]. Figure 2(e) shows that the MTF of shadowgraphy without the scattering medium is optimal. This measurement provides a reference for comparison and shows that the maximum resolvable spatial frequencies are almost 50 line pairs per millimeter (lp/mm). When the imaging object is hidden behind the scattering medium, the MTF values for shadowgraphy are reduced to less than 0.2. For OKG ballistic imaging, the MTF values at low spatial frequency are significantly better than those for shadowgraphy because of the filtering of scattered photons. However, the values become too low when the object's spatial frequency exceeds 15 lp/mm because of the low-pass filtering influence. Because the femtosecond DOKG imaging not only filters scattered photons but also overcomes the low-pass filtering influence, its MTF values are nearly as high as those of the reference image at low spatial frequency, as shown in Fig. 2(e). Even when the spatial frequency increases, the image contrasts for DOKG ballistic imaging gradually decrease but still are obviously larger than those for the OKG ballistic imaging. Figure 2(f) shows that the PSF of reference imaging has narrowest full width at half maximum (FWHM). When the scattering medium is added to the optical train, the PSF broadens severely. When OKE gating is added to the experimental configuration, the PSF shrinks and the PSF of DOKG is the curve closest to the reference. The images of the resolution test target, the MTF and the PSF all reveal the same characteristics of the three imaging methods.

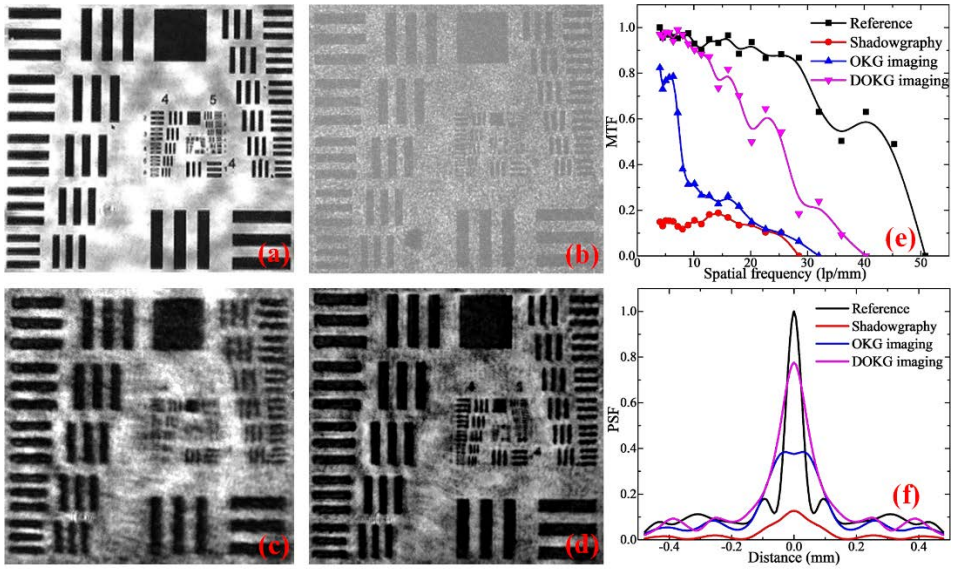


Fig. 2. Images obtained by different imaging methods through the scattering medium and their MTF and PSF — (a) reference image: shadowgraphy results without scattering medium; (b) shadowgraphy results with scattering medium; (c) OKG imaging with scattering medium; (d) DOKG imaging with scattering medium; and (e) MTF of the imaging system; (f) PSF of the imaging system.

Optics EXPRESS

It's noted that the periodical bars on the resolution test target may lead to Talbot effect which means that repetitive slits are said to make repetitive images of themselves in our experimental configuration [21]. The self-images with offset in the lateral direction which are new objects for imaging system may affect the contrast and resolution of the final image. For the imaging targets of any size in our experimental configuration, the basic unit for Talbot length is much larger than the depth of field. For example, the basic unit for Talbot length of the targets comparable in size to the limit resolution is about 0.05mm. The depth of field for the same targets is about 0.026mm, which means that the self-image seen as new object will have little effect on the final image. So we ignore the Talbot effect in shadowgraphy.

To further analyze the quantitative frequency characteristics we compared the power spectra obtained with the three different techniques by processing the Figs. 2(a)-2(d). The center of the power spectra represents the low frequency component and the surrounding represents the high frequency component. We focus on the power spectral intensity on the x and y axes because all the resolution test patterns are horizontal and vertical. The power spectral intensity on the axes of the reference is high as shown in Fig. 3(a). When the scattering medium is added to the optical train, the intensities of the effective frequencies decrease significantly and severe high frequency noises are introduced into the power spectra as shown in Fig. 3(b). OKG imaging help filtering out some high frequency noises and improve the signal-to-noise ratio of low frequency components as shown in Fig. 3(c). DOKG imaging further improve the signal-to-noise ratio of moderate and high frequency components compared with OKG imaging as shown in Fig. 3(d).

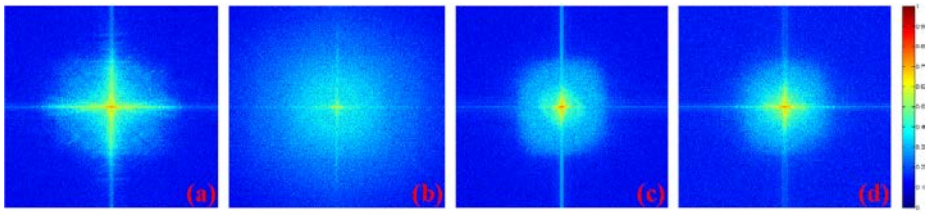


Fig. 3. Power spectra obtained with (a) reference image; (b) shadowgraphy; (c) OKG imaging; (d) DOKG imaging.

Furthermore, these three femtosecond imaging methods for measurements of flow structures in liquid-gas mixed sprays were compared. Figures 4(a) and 4(b) show images of liquid-gas spray simultaneously obtained by using the femtosecond shadowgraphy and OKG ballistic imaging. Figure 4(c) shows images obtained by the femtosecond DOKG ballistic imaging. Figures 4(a) and 4(b) show that most information of the liquid-gas spray structures, such as curvature of the big liquid structure, ligament length, and droplet distribution, can be captured by using the femtosecond shadowgraphy due to freezing the motion of the spray structure. However, the magnified view on the right side in Fig. 4(a) shows that some spray structures are still blurred, even inauthentic, compared with those shown in the magnified view on the right side in Fig. 4(b). Specifically, the magnified view of simultaneous comparison in Figs. 4(a)-I and 4(b)-I shows that some tiny droplets eroded by scattered photons in the femtosecond shadowgraphy can be distinguished in the femtosecond OKG ballistic imaging. Figures 4(a)-II and 4(b)-II show a comparison of the same ligament structure, where the edge structure in OKG imaging is significantly sharper, but the ligament edge in the femtosecond shadowgraphy is full of burr structures. Figures 4(a)-III and 4(b)-III compare the big liquid sheet in sprays. There are some bright and gray spots in the femtosecond shadowgraphy images, but they do not exist in the femtosecond OKG ballistic images.

This phenomenon can be attributed to the scattered photons, which lose their original direction of propagation and eventually appear in the wrong places of the CCD. These scattered photons destroyed the original shape of the spray structure in the images obtained by using the femtosecond shadowgraphy. That is why there are many bright spots on the edge and inside of

Optics EXPRESS

the spray structure in Fig. 4(a). As the OKG ballistic imaging simultaneously has the ability of filtering scattered photons and freezing the spray motion, it can image minor droplets, clearer edges of ligament structures, and more-realistic liquid sheet structures. To further enhance the comparison, the Figs. 4(a)-I and 4(b)-I were processed using the maximum entropy threshold segmentation method [22] as shown in Figs. 4(d) and 4(e). The two-level images show that many speckles caused by scattered photons appear on the edge and inside of the small spray structures, which affects the authenticity of spray imaging. The results shown in Figs. 4(a) and 4(b) also indicate that, if the spray is not optically dense enough for the scattered photons to have little eroding effect, it is advisable to measure the characteristics of the liquid-gas mixed spray using femtosecond shadowgraphy, which has a simple experimental setup. However, if the spray is optically dense enough, it is advisable to measure the characteristics of the liquid-gas mixed spray using femtosecond OKG ballistic imaging, which can mitigate the multiple scattering noise.

Although femtosecond OKG ballistic imaging has advantages compared with femtosecond shadowgraphy, its spatial resolution is still limited because of the low-pass spatial-filtering influence described above. To overcome further the low-pass spatial-filtering influence of the OKG ballistic imaging, the femtosecond DOKG ballistic-imaging approach was employed to image the liquid-gas mixed sprays. The experimental arrangement of the DOKG is shown in Fig. 1(b). Spray conditions, including water flow rate, air flow rate, and the exit diameter of the nozzle, are still the same as those mentioned above. The images obtained by the femtosecond DOKG ballistic images shown in Fig. 4(c)-I and 4(c)-II show that the edges of spray structures are sharper than those for the OKG ballistic imaging. Figure 4(c)-III shows the tiny droplets more clearly. Because the femtosecond DOKG ballistic imaging cannot only freeze the spray motion and filter scattered photons but also remove the background light and compensate for the high-spatial-frequency components, it can image the spray structures with high contrast and high spatial resolution. However, femtosecond DOKG ballistic imaging has more-complicated experimental arrangements and image processing. It is suitable for imaging optical dense spray with many tiny structures.

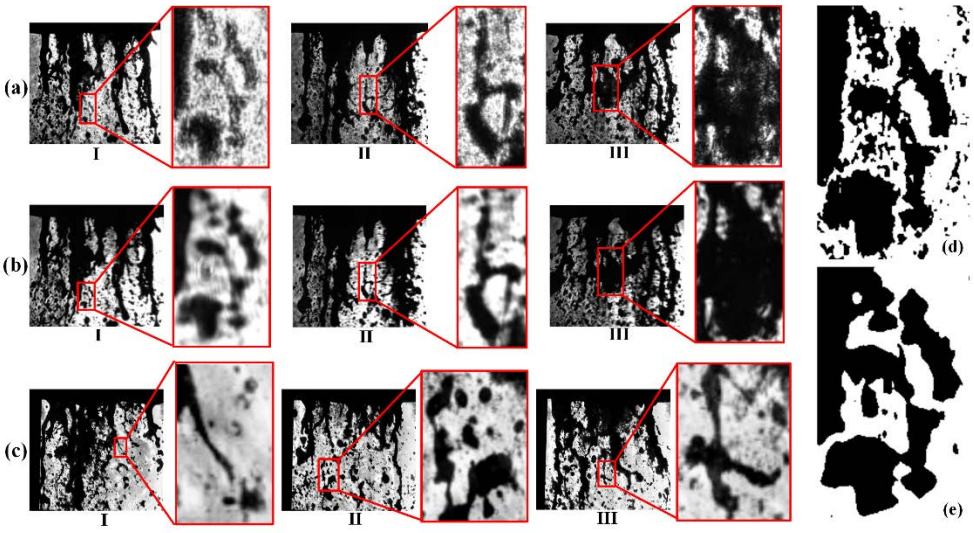


Fig. 4. Images of liquid-gas spray obtained by different methods of imaging and their partial enlargements: (a) shadowgraphy, (b) OKG imaging, and (c) DOKG imaging. (d) and (e): Picture segmentation results of the enlargements of Figs. 4(a)-I and 4(b)-I.

Optics EXPRESS

## 4. Conclusions

In conclusion, three ultrafast imaging methods were compared to image liquid-gas sprays. The image contrasts of the three imaging systems were quantitatively calculated for imaging a static object hidden in the scattering medium. The results show that OKG ballistic imaging can significantly improve the image contrasts and DOKG ballistic imaging can further enhance the image contrast at a high spatial frequency. From the simultaneous comparisons in liquid-gas mixed sprays, it can be seen that most of the spray structures were captured using femtosecond shadowgraphy because of its freezing the motion of the high-speed sprays. The finer droplets, shaper edges of ligaments, and more-realistic liquid sheets were captured using the OKG ballistic imaging method by filtering multiple scattered photons. This indicated that, if the spray is relatively dilute in which the scattered photons have little eroding effect, femtosecond shadowgraphy whose experimental setup is simple is an advantageous method. However, if the spray has high optical depth, in which huge amounts of scattered photons are produced, OKG ballistic imaging is suggested to measure the characteristics of the spray. DOKG ballistic imaging further improved the sharpness of the edges and showed the tiny droplets more clearly compared with OKG ballistic imaging. However, its experimental setup and image processing are more complicated. It is suitable for imaging optically dense spray with many tiny structures.

## Funding

National Natural Science Foundation of China (NSFC) (61690221 and 61427816); Natural Science Basic Research Plan in Shaanxi Province of China (2018JM6012).

## References

1. J. B. Schmidt, Z. D. Schaefer, T. R. Meyer, S. Roy, S. A. Danczyk, and J. R. Gord, "Ultrafast time-gated ballistic-photon imaging and shadowgraphy in optically dense rocket sprays," Appl. Opt. **48**(4), B137–B144 (2009).
2. H. Purwar, H. Wang, M. Tang, S. Idlahcen, C. Rozé, J. B. Blaisot, T. Godin, and A. Hideur, "Ultrafast high-repetition imaging of fuel sprays using picosecond fiber laser," Opt. Express **23**(26), 33396–33407 (2015).
3. D. Sedarsky, M. Paciaroni, E. Berrocal, P. Petterson, J. Zelina, J. Gord, and M. Linne, "Model validation image data for breakup of a liquid jet in crossflow part I," Exp. Fluids **49**(2), 391–408 (2010).
4. M. Linne, "Imaging in the optically dense regions of a spray: A review of developing techniques," Prog. Energy Combust. Sci. **39**(5), 403–440 (2013).
5. Y. Zheng, W. Tan, X. Liu, and J. Tong, "Ballistic imaging through an intense scattering medium using a supercontinuum with a roundabout spatial gate," Opt. Express **25**(17), 20431–20436 (2017).
6. M. Rahm, Z. Falgout, D. Sedarsky, and M. Linne, "Optical sectioning for measurements in transient sprays," Opt. Express **24**(5), 4610–4621 (2016).
7. L. Wang, P. P. Ho, C. Liu, G. Zhang, and R. R. Alfano, "Ballistic 2-d imaging through scattering walls using an ultrafast optical kerr gate," Science **253**(5021), 769–771 (1991).
8. L. Wang, P. P. Ho, X. Liang, H. Dai, and R. R. Alfano, "Kerr - Fourier imaging of hidden objects in thick turbid media," Opt. Lett. **18**(3), 241–243 (1993).
9. P. A. Galland, X. Liang, L. Wang, K. Breisacher, L. Liou, P. P. Ho, and R. R. Alfano, *Time-resolved optical imaging of jet sprays and droplets in highly scattering medium* (American Society of Mechanical Engineers, 1995).
10. M. Paciaroni and M. Linne, "Single-shot, two-dimensional ballistic imaging through scattering media," Appl. Opt. **43**(26), 5100–5109 (2004).
11. M. Linne, M. Paciaroni, T. Hall, and T. Parker, "Ballistic imaging of the near field in a diesel spray," Exp. Fluids **40**(6), 836–846 (2006).
12. M. A. Linne, M. Paciaroni, J. R. Gord, and T. R. Meyer, "Ballistic imaging of the liquid core for a steady jet in crossflow," Appl. Opt. **44**(31), 6627–6634 (2005).
13. M. Linne, D. Sedarsky, T. Meyer, J. Gord, and C. Carter, "ballistic imaging in the near-field of an effervescent spray," Exp. Fluids **49**(4), 911–923 (2010).
14. S. Idlahcen, C. Rozé, L. Méès, T. Girasole, and J. B. Blaisot, "Sub-picosecond ballistic imaging of a liquid jet," Exp. Fluids **52**(2), 289–298 (2012).
15. M. Linne, M. Rahm, and Z. Falgout, "Correlation of Internal Flow and Spray Breakup for a Fuel Injector Used in Ship Engines," The 8th US National Combustion Meeting (Combustion Instituute, 2013), paper 070HE-0032.
16. S. Duran, J. Porter, and T. E. Parker, "Ballistic Imaging of Sprays at Diesel Relevant Conditions," in Proceedings of the Twelfth International Conference on Liquid Atomisation and Spray Systems (ICLASS), Heidelberg, Germany, 2–6 Sept. 2012.

Optics EXPRESS

17. Y. Ren, J. Si, W. Tan, S. Xu, J. Tong, and X. Hou, "Microscopic imaging through a turbid medium by use of a differential optical Kerr Gate," IEEE Photonics Technol. Lett. **28**(4), 394–397 (2016).
18. M. E. Orczyk, M. Samoc, J. Swiatkiewicz, and P. N. Prasad, "Dynamics of third-order nonlinearity of canthaxanthin carotenoid by the optically heterodyned phase-tuned femtosecond optical Kerr gate," J. Chem. Phys. **98**(4), 2524–2533 (1993).
19. G. C. Cheng, R. Cohn, C. Johnson, R. R. Davis, and J. A. Muss, "Development of GOX/Kerosene Swirl Coaxial Injector Technology," in 39th AIAA/ASME/SAE/ASEE Joint Propulsion Conference and Exhibit. (Aerospace Research Central, 2003), paper 4751.
20. P. Zhan, W. Tan, J. Si, S. Xu, J. Tong, and X. Hou, "Optical imaging of objects in turbid media using heterodyned optical Kerr gate," Appl. Phys. Lett. **104**(21), 211907 (2014).
21. P. Latimer and R. F. Crouse, "Talbot effect reinterpreted," Appl. Opt. **31**(1), 80–89 (1992).
22. J. N. Kapur, P. K. Sahoo, and A. K. C. Wong, "A new method for gray-level picture thresholding using the entropy of the histgram," Comput. Vis. Graph. Image Process. **29**(3), 223–237 (1985).